Generation of Broadband Supercontinuum and Isolated Attosecond Pulse in a Chirped Two-Colour Laser Field

Gang-Tai Zhang

Department of Physics and Information Technology, Baoji University of Arts and Sciences, Baoji 721016, China

Reprint requests to G.-T. Z.; E-mail: gtzhang79@163.com

Z. Naturforsch. **68a,** 461 – 474 (2013) / DOI: 10.5560/ZNA.2013-0024
Received November 20, 2012 / revised February 6, 2013 / published online May 1, 2013

We present a theoretical investigation of high-order harmonic generation in a chirped two-colour laser field, which is synthesized by an 800 nm fundamental chirped pulse and a 1200 nm subharmonic chirped pulse. With the introduction of a polarization angle, both the harmonic cutoff is significantly extended and the spectrum intensity is effectively enhanced compared with the orthogonally polarized chirped two-colour field. When the polarization angle between the two chirped pulses is less than or equal to 0.27π, the broadband supercontinuum with a single quantum path contribution is achieved, and then isolated attosecond pulses with the duration of about 40 as are directly obtained, which are all linearly polarized. In addition, the influences of other laser parameters on the supercontinuum are also investigated.

Key words: High-Order Harmonic Generation; Isolated Attosecond Pulse; Supercontinuum; Chirped Two-Colour Laser Field.

1. Introduction

Attosecond (as) extreme ultraviolet (XUV) pulses open a way to study and operate basic ultrafast electronic processes in atoms and molecules with unprecedented accuracy and resolution [1 – 3]. Since high-order harmonic generation (HHG), which is induced by the interaction of a high-intensity laser pulse with atoms or molecules, enables the production of ultrashort radiation at the attosecond time scale, the attosecond pulse generation based on HHG has attracted a large amount of attention. The HHG process can be well understood by the three-step model [4]: ionization, acceleration, and recombination. During the recombination, a photon is emitted with the maximum photon energy given by E_{cutoff} [eV] $= I_{\mathrm{p}} + 3.17U_{\mathrm{p}}$, where I_{p} is the atomic ionization potential and U_{p} [eV] $= 9.38 \times 10^{-14} I$ [W/cm^2](λ [μm])^2 is the ponderomotive energy of the electron in the laser field. For a long laser pulse, this process usually occurs at every half optical cycle of the laser field and generates an attosecond pulse train (APT) including two attosecond pulses in each optical cycle. But for practical application, an isolated attosecond pulse is more useful than a chain of attosecond pulses, hence much effort has been paid out to extract an isolated attosecond pulse. It has been shown that an isolated attosecond pulse can be generated by using the phase-stabilized few-cycle laser pulse [1, 2, 5], the multicycle driver pulses [6], the polarization gating scheme [3, 7, 8], the polarization gating technique combined with the ionization dynamics and the spatial filtering [9], the two-colour mixing method [10 – 12], and quantum path control [13 – 15]. In a recent breakthrough work, an isolated 80 as pulse was realized in a recent experiment [16]. Zhao et al. [17] reported on the generation of a single isolated 67 as pulse, which is the shortest attosecond pulse to the best of our knowledge, from an extreme UV supercontinuum covering 55 – 130 eV generated by the double optical gating technique. However, the duration of isolated attosecond pulses is still far greater than one atomic unit of time (i.e., 24 as). It has been suggested that the bandwidth of the attosecond pulse is more important than the duration in attosecond science [18]. Therefore, it is an urgent need to generate isolated attosecond pulses with broader bandwidth and shorter pulse duration.

In addition, from the cutoff law, one can see clearly that the harmonic cutoff can be extended through enhancing the intensity of the driving field or using

a longer-wavelength laser for the driving field, since the ponderomotive energy is proportional to the intensity of the driving field or the square of the wavelength of the driving field. However, on the one hand, too high driving field will result in the ionization saturation of the target atom and limit the harmonic yields; on the other hand, high ionization rate also leads to plasma defocusing of the driving pulse and dephasing of the atomic dipole oscillators, then further decreases the conversion efficiency. Therefore, an efficient method for significantly extending the harmonic cutoff is to adopt a longer-wavelength driving field. With the rapid development of ultrafast laser technology, mid-infrared (IR) laser pulses with high intensity level can be produced by high-power femtosecond optical parametric amplifiers (OPAs) [19, 20]. Takahashi et al. [21] experimentally showed that by using the mid-IR pulse at wavelength of 1.6 μm the maximum harmonic photon energies attained are 300 and 450 eV in neon and helium, respectively. Popmintchev et al. [22] showed that bright high-harmonic X-ray supercontinua with photon energies spanning from the extreme ultraviolet to 1.6 keV (< 7.7 Å) are generated by focusing 3.9 μm wavelength pulses from a tabletop femtosecond laser into a waveguide filled with helium gas. Tate et al. [23] has theoretically shown that a mid-IR driving pulse not only produces much more energetic harmonic photons but also reduces harmonic chirps, which is helpful to the attosecond pulse generation.

As is well known, the HHG process is highly dependent on the ellipticity of the driving laser field. The time-varying polarization gating is a very important technique to generate broadband XUV supercontinuum and isolated attosecond pulses. Sansone et al. [3] demonstrated the generation of a single 130 as pulse by rapidly sweeping the laser polarization state within an optical cycle. Tzallas et al. [24] presented a novel approach for intense broadband EUV continuum generation using a high-intensity, many-cycle, IR pulsed laser through the interferometric modulation of the ellipticity of 50 fs-long driving pulses, and they also realized a single attosecond pulse with a minimum duration of 340 as using a silicon filter transmitting between 55 and 32 nm. Kitzler et al. [25] showed that the time varying polarization field synthesized by two orthogonally polarized pulses can be used for producing an attosecond pulse train. Altucci et al. [26] implemented a new experimental scheme for the generation of single-shot EUV continua that exploits a combination of transform-limited 15 fs, 800 nm pulses and chirped 35 fs, 800 nm pulses with orthogonal polarizations. By using an orthogonal two-colour laser field consisted of a 9 fs/800 nm pulse in x-direction and a 9 fs/1300 nm pulse in y-direction, Yu et al. [27] theoretically demonstrated the generation of a single 115 as pulse. Moreover, they also investigated the single attosecond pulse generation from aligned molecules using two-colour polarization gating and obtained an isolated 83 as pulse after the linear chirp compensation [28]. By combining a few-cycle driving pulse with its second-harmonic field at a polarization angle of $\pi/3$, Hong et al. [29] generated an isolated 100 as pulse with high signal-to-noise ratio. Yao et al. [30] theoretically demonstrated that by optimization of the angle in-between polarization planes of two linearly polarized pulses, a broad XUV supercontinuum with a fairly good conversion efficiency and an isolated 73 as pulse can be achieved with a multicycle two-colour laser field, and they also demonstrated the generation of wavelength-tunable, narrow-bandwidth XUV radiation by HHG driven by an orthogonally polarized two-colour laser field, which is composed of a 10 fs, 1500 nm laser pulse and a 40 fs, 2400 nm laser pulse [31].

Recent research results have been shown that HHG is sensitive to the chirp of driving laser pulses [32 – 37]. With this controlling technique, some authors have successfully synthesized broadband isolated attosecond pulses, such as an isolated 108 as pulse via coherent control of an intense few-cycle chirped laser pulse [32], a single 58 as pulse using a chirped few-cycle laser and static electric field [33], an isolated 26 as pulse using an intense few-cycle chirped laser and its high-order harmonic pulses [34], an isolated 38 as pulse using an intense few-cycle linearly chirped laser and a subharmonic laser pulse [35], an isolated 57 as pulse with a chirped two-colour laser field [36], and an isolated 31 as pulse using two-colour laser pulses with the combined chirp effects [37].

In this paper, the motivation of our simulation lies in the following considerations: first, from the works mentioned above, it is important to accurately control the polarization angle between the two laser pulses to obtain a broadband supercontinuum. However, in our simulation we find that the broadband supercontinuum with high conversion efficiency can be produced in a wide range of polarization angle values, which is beneficial for the generation of an ultrashort isolated attosecond pulse. Second, using an exact numerical solu-

tion of the time-dependent Schrödinger equation, Kitzler et al. [38] demonstrated two examples of coherent measurement methods which are based on the polarization sweep of harmonic radiation created by orthogonally polarized two-colour laser fields. Thereinto, the first example is the creation of high harmonic attosecond pulse trains which can be used just as if they were a single attosecond pulse. Howbeit, in this paper, by applying the Lewenstein model, we exploit the combined effects of a chirp two-colour laser field and a polarization angle to study the generation of intense isolated attosecond pulses, as we will discuss below. Third, little research has been reported in the chirped two-colour laser field with a polarization angle. Due to these reasons, in this paper we theoretically investigate the HHG and attosecond pulse generation in a chirped two-colour laser field with a polarization angle. The numerical result shows that for the polarization angle of $\theta \leq 0.27\pi$, since the supercontinuum with high conversion efficiency covers an extremely broad bandwidth and is mainly originated from a single quantum path contribution, intense isolated attosecond pulses with the duration of about 40 as are directly obtained, which are linearly polarized. In addition, we investigate the influences of the laser intensity and chirped parameter on the supercontinuum. We also show that this scheme can work in the multicycle regime.

2. Theoretical Model and Method

In our scheme, a 5 fs/800 nm fundamental chirped pulse and a 10 fs/1200 nm subharmonic chirped pulse are employed for synthesizing a chirped two-colour laser field. The model atom is neon with 21.56 eV of the ionization energy for the ground state. The intensities of the two chirped pulses are chosen to be $5\cdot10^{14}$ W/cm^2 and $2\cdot10^{14}$ W/cm^2, respectively. The electric field of the synthesized laser pulse along the x- and y-directions can be expressed, respectively, as

$$E_x(t) = E_1 f_1(t)\cos[\omega_1 t + \delta_1(t)]\sin\theta\,, \tag{1}$$

$$E_y(t) = E_1 f_1(t)\cos[\omega_1 t + \delta_1(t)]\cos\theta + E_2 f_2(t)\cos[\omega_2 t + \delta_2(t)]\,, \tag{2}$$

where $\delta_i(t)$ $(i=1,2)$ are the time profiles of the carrier envelope phases (CEPs), which have the time-varying hyperbolic tangent form $\delta_i(t) = -\beta_i \tanh[(t-t_i)/T_i]$ $(i=1,2)$. The chirp form is controlled by adjusting the two parameters β_i and T_i $(i=1,2)$, and t_i $(i=1,2)$ are used to adjusted the sweep range. Due to the recent advancement of comb laser technology [32, 39, 40], it is highly likely that such a time-varying CEP can be achieved in the near future. E_i and ω_i $(i=1,2)$ are the amplitudes and frequencies of the 800 nm fundamental chirped pulse and the 1200 nm subharmonic chirped pulse, respectively. $f_i(t) = \exp[-4\ln 2(t/\tau_i)^2]$ $(i=1,2)$ are the envelope functions and τ_i $(i=1,2)$ are the corresponding pulse durations of the two chirped pulses. θ is the polarization angle between the two chirped pulses. In the present work, T_i and t_i $(i=1,2)$ are fixed at 200 a.u. and 0, respectively, and $\beta_1 = 6.25$ and $\beta_2 = 4$ are adopted. The three-dimension (3D) plot of the chirped two-colour laser field is shown in Figure 1.

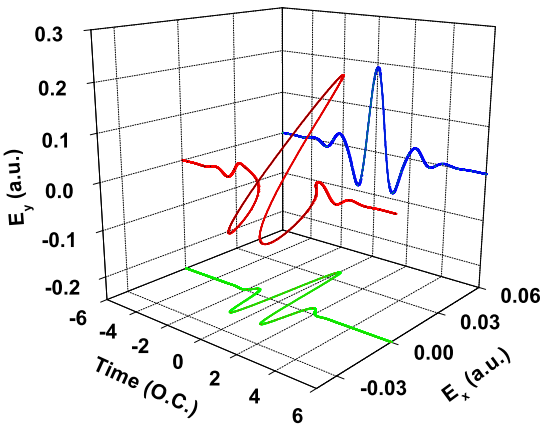

Fig. 1 (colour online). 3D plot of the chirped two-colour laser field synthesized by a 5 fs/800 nm fundamental chirped laser pulse ($\beta_1 = 6.25$) and a 10 fs/1200 nm subharmonic chirped laser pulse ($\beta_2 = 4.0$). The intensities of the two chirped pulses are chosen to be $5\cdot10^{14}$ W/cm^2 and $2\cdot10^{14}$ W/cm^2, respectively.

In our calculation, the HHG spectrum can be qualitatively studied by the non-adiabatic Lewenstein model [41], which is based on a single-active electron approximation and has been widely employed. In this model, the instantaneous dipole moment of an atom is described as (atomic units are used),

$$d_{\rm nl}(t) = i\int_{-\infty}^{t} {\rm d}t' \left[\frac{\pi}{\varepsilon + i(t-t')/2}\right]^{3/2} \cdot d^*[p_{\rm st}(t',t) - A(t)]\cdot d[p_{\rm st}(t',t) - A(t')] \cdot \exp[-iS_{\rm st}(t',t)]E_f(t')g(t') + {\rm c.c.}\,, \tag{3}$$

here $E_f(t)$ is the electric field of the laser pulse, $A(t)$ is its associated vector potential, and ε is a positive regularization constant. $p_{\rm st}$ and $S_{\rm st}$ are the stationary values

of the momentum and quasi-classical action, respectively, which are shown as follows:

$$p_{\mathrm{st}}(t',t) = \frac{1}{t-t'}\int_{t'}^{t} A(t'')\,\mathrm{d}t'', \tag{4}$$

$$S_{\mathrm{st}}(t',t) = (t-t')I_{\mathrm{p}} - \frac{1}{2}p_{\mathrm{st}}^2(t',t)(t-t') + \frac{1}{2}\int_{t'}^{t} A^2(t'')\,\mathrm{d}t'', \tag{5}$$

where I_{p} denotes the ionization energy of the atom. $d(p)$ is the dipole matrix element for bound-free transitions. For hydrogen-like atoms, it can be approximated as

$$d(p) = i\frac{2^{7/2}}{\pi}(2I_{\mathrm{p}})^{5/4}\frac{p}{(p^2+2I_{\mathrm{p}})^3}. \tag{6}$$

$g(t)$ in (3) represents the ground amplitude:

$$g(t') = \exp[-\int_{-\infty}^{t'} w(t'')\,\mathrm{d}t''], \tag{7}$$

where $w(t'')$ is the ionization rate and is calculated by the Ammosov–Delone–Krainov (ADK) tunnelling model [42].

The harmonic spectrum $P_A(q\omega_{\mathrm{l}})$ is obtained by Fourier transforming the time-dependent dipole acceleration $a(t)$ of a model atom:

$$P_A(q\omega_{\mathrm{l}}) = \left|\frac{1}{\sqrt{2\pi}}\int_0^T a(t)\,\mathrm{e}^{\mathrm{i}q\omega_{\mathrm{l}}t}\,\mathrm{d}t\right|^2, \tag{8}$$

where $a(t) = \ddot{d}_{\mathrm{nl}}(t)$, T and ω_{l} are the duration and frequency of the driving pulse, respectively. q represents the harmonic order.

To study the detailed spectral and temporal structures of HHG, we perform the time–frequency analysis by means of the wavelet transform [43],

$$A(t_0,\omega_{\mathrm{l}}) = \int a(t)\sqrt{\omega_{\mathrm{l}}}W(\omega_{\mathrm{l}}(t-t_0))\,\mathrm{d}t, \tag{9}$$

where $W(\omega_{\mathrm{l}}(t-t_0))$ is the mother wavelet expressed as

$$W(x) = \left(\frac{1}{\sqrt{\tau}}\right)\mathrm{e}^{\mathrm{i}x}\,\mathrm{e}^{-x^2/2\tau^2}, \tag{10}$$

and $\tau = 30$ in our calculations.

Finally, by superposing several orders of harmonics, an attosecond pulse is generated and the temporal profile of the attosecond pulse is

$$I(t) = \left|\sum_q a_q\,\mathrm{e}^{\mathrm{i}q\omega_{\mathrm{l}}t}\right|, \tag{11}$$

where $a_q = \int a(t)\,\mathrm{e}^{-\mathrm{i}q\omega_{\mathrm{l}}t}\,\mathrm{d}t$.

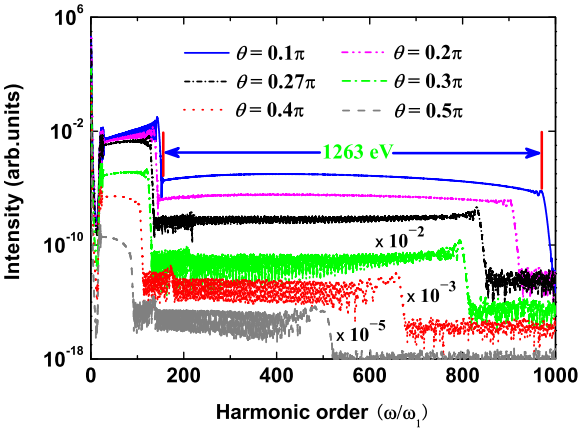

Fig. 2 (colour online). Harmonic spectra in the chirped two-colour laser field with different polarization angles of 0.1π, 0.2π, 0.27π, 0.3π, 0.4π, and 0.5π, respectively. For the purpose of clarity, the harmonic intensities for $\theta = 0.3\pi$, $\theta = 0.4\pi$, and $\theta = 0.5\pi$ are multiplied by factors of 10^{-2}, 10^{-3}, and 10^{-5}, respectively. Other parameters are the same as those in Figure 1.

3. Results and Discussion

We first investigate the HHG spectra in the chirped two-colour laser field with different polarization angles. The intensity of the harmonic spectrum generated in the chirped two-colour field is obtained by summing up the intensity of the x-component and the y-component of the harmonics. Figure 2 is the harmonic spectra for the cases of five different polarization angles of 0.1π, 0.2π, 0.27π, 0.3π, 0.4π, and 0.5π, respectively. Other parameters are the same as those in Figure 1. Because the harmonic spectrum in the plateau region has overlap, we shift three curves for the cases of 0.3π, 0.4π, and 0.5π for the purpose of clarity so that the harmonic signals for 0.3π, 0.4π, and 0.5π are scaled. Indeed, the spectral intensities of 0.3π, 0.4π, and 0.5π decrease in sequence. At first glance, for the cases of all polarization angles, a very prominent feature of the spectra shown in Figure 2 is the appearance of a two-plateau structure with two pronounced cutoffs. (Actually, for the case of the polarization angle above 0.3π, the harmonic spectrum presents a three-plateau structure, however the difference of the harmonic intensity between the first and second plateaus is not so great, so the three-plateau structure can be taken as a two-plateau one.) The second plateau is several orders weaker than the first plateau, which is

caused by the lower ionization rate of the corresponding electron. From Figure 2, one can see clearly that the harmonic spectrum is sensitive to the variation of the polarization angle. As the polarization angle between the two chirped pulses increases, the harmonic intensity decreases rapidly, and the spectral cutoff becomes shorter, which also reduces the bandwidth of the supercontinuum. Contrarily, as the polarization angle decreases, the spectral cutoff and the harmonic efficiency are enhanced, especially for the case of $\theta = 0.1\pi$, where the harmonic cutoff reaches 969th order, resulting in an ultrabroad supercontinuum (i.e., the region in the second plateau) with a 1263 eV bandwidth. Moreover, the spectrum modulation becomes stronger and stronger with the increase of the polarization angle. This is due to that there are two major quantum paths with nearly equal intensity contributing to the plateau harmonic, causing more obvious interference structure. Note that when the polarization angle is less than or equal to 0.27π, we find that the broadband supercontinuum with less modulation and high conversion efficiency can be achieved in contrast with the orthogonally polarized chirped two-colour field, which is better for producing an intense ultrashort isolated attosecond pulse.

In order to go deep into the spectrum structure, we take the cases with $\theta = 0.1\pi$ and $\theta = 0.5\pi$ as examples to investigate the emission times of the harmonics by using the time–frequency analysis method. As shown in Figures 3a and 3b, there are three peaks (marked as A_1, B_1, and C_1) contributing to the harmonics. The maximum orders of A_1, B_1, and C_1 are approximately 135th, 510th, and 92nd, respectively. The intensity of C_1 is the strongest in the three peaks, and the intensities of A_1 and B_1 are comparable but weaker than that of C_1, in other words, the harmonic yield of C_1 is higher than that of the two other peaks, resulting in a double-plateau structure as shown by the dashed gray curve in Figure 2. Furthermore, the harmonics higher than 135th order are mainly contributed by B_1, forming a supercontinuum with the bandwidth of 582 eV. However, for these harmonics beyond 135th order, since there are two quantum paths with different emission times and comparable intensities contributing to the same harmonic, the interference between these quantum paths leads to the strong modulation for the plateau harmonics. For the harmonics near the cutoff, the short and long quantum paths are merged into one with equivalent emission time, and the harmonics are synchronically emitted, i.e., well phase-locked. (The phase locking means that the phase difference between consecutive harmonics is constant, so that the emission time is equal for these harmonics, i.e., the harmonics are synchronically emitted.) However, the width of these harmonics with one quantum path contribution is very narrow, which can synthesize an isolated 104 as pulse according to our calculation. Hereinafter, we will give the calculated results. Figures 3c and 3d show the time–frequency distributions of the x- and y-component of the HHG spectrum for the field shown in Figure 1, respectively. Clearly, there are three peaks with the maximum harmonic orders of about 255, 969, and 155 contributing to the HHG for both components, which are marked as A_2, B_2, and C_2, respectively. The peak A_2 is at about -0.63 o.c., but the peak intensity is weaker than that of the peaks B_2 and C_2 for both components, thus their contributions to the HHG can be ignored. In addition, C_2 is stronger than B_2 in the harmonic intensity for both components, which is the reason for the double-plateau structure in the spectrum shown by the solid blue curve in Figure 2. Compared with the orthogonally chirped two-colour field, the intensities of the peaks B_2 and C_2, which mainly contribute to the HHG emission, are higher than that of the peaks A_1 and B_1 in Figures 3a and 3b. This indicates that the harmonic yield in the field shown in Figure 1 is much more efficient and also explains why the conversion efficiency of the HHG can be effectively improved. The peak B_2 is at approximately -0.5 o.c., corresponding to the 969th harmonic order (1503 eV). Since the highest harmonic order in the field adopted in Figure 1 is much more higher than that in the orthogonally polarized chirped two-colour field, the spectral cutoff for the case is greatly extended. The peak C_2 is at about 1.54 o.c., corresponding to the 155th harmonic order (240 eV). Thus the harmonics higher than 155th order only originate from the contribution of B_2, forming a broad XUV supercontinuum with a 1263 eV bandwidth, which is in agreement with the solid blue curve in Figure 2. Moreover, the energy difference between the two peaks (B_2 and A_2) is much larger than that using two-colour chirped field with orthogonal polarization, which is responsible for the generation of the broadband supercontinuum using the two-colour chirped field with the polarization angles of 0.1π. Further, for the peak B_2, though there are two dominating quantum paths contributing to the same harmonic, the contribution of the short path is much higher than that

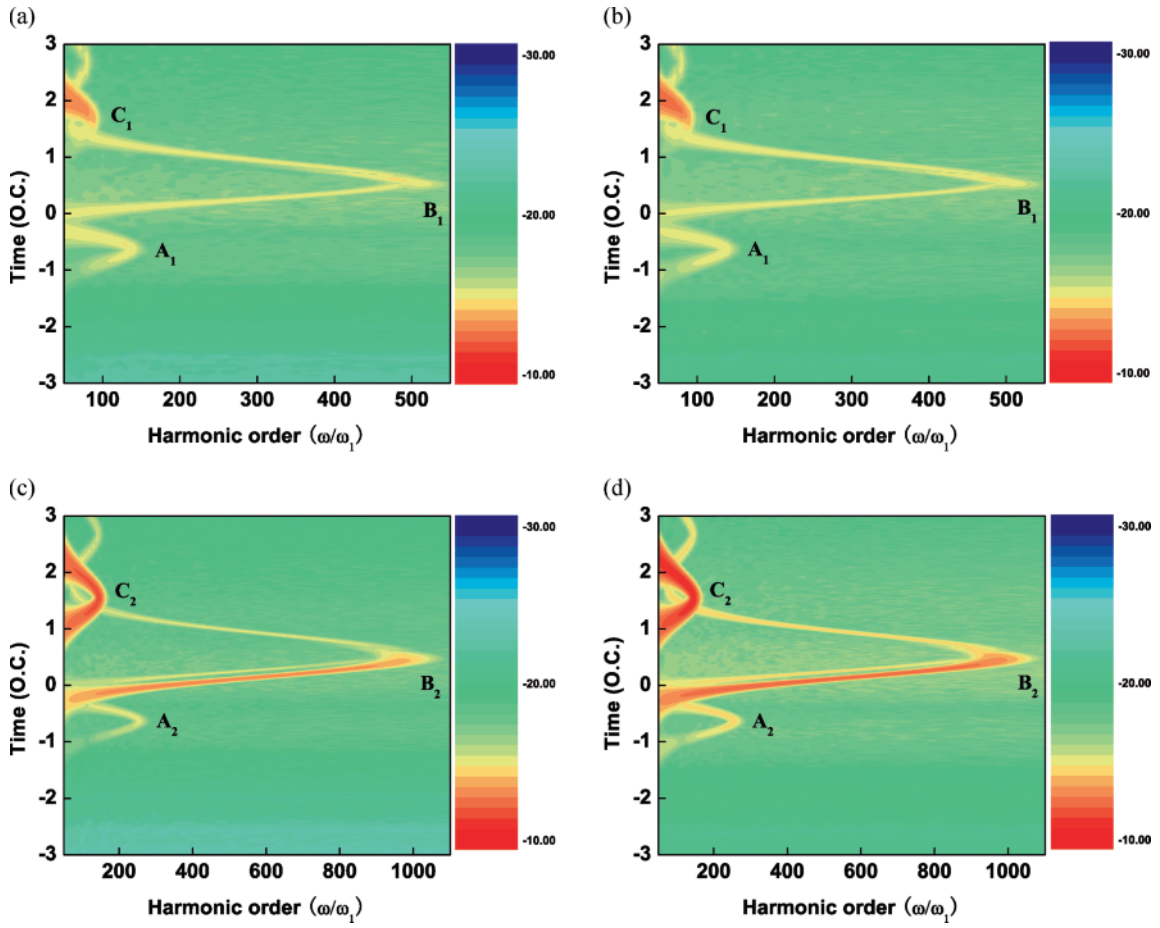

Fig. 3 (colour online). Time–frequency distributions of (a) *x*-component and (b) *y*-component of the HHG spectrum for the orthogonally polarized chirped two-colour field. (c) and (d): The same as (a) and (b) but for the laser field shown in Figure 1.

of the long one, i.e., the short-path harmonics are effectively selected for both components. For other polarization angle, i.e., $\theta \leq 0.27\pi$, we find that similar results are obtained in terms of time–frequency analyses of the dipole response.

Figure 4 illustrates the electron dynamics of the HHG process and the ionization rate in the two-colour chirped field with the polarization angle of 0.1π. Since the electric field strength of the *x*-direction is much weaker than that of the *y*-direction for the relatively small polarization angle, we can take the *y*-direction as an example to explore the underlying physics of the extension of both the spectral cutoff and the supercontinuum, as well as the enhancement of the harmonic efficiency. For comparison, the inset in Figure 4b shows the ionization rate in the orthogonally chirped two-colour field. Figure 4b shows the dependence of the harmonic order on the ionization (green diamonds) and the emission times (red circles) and the tunnel ionization rate (gray filled curve), respectively. As shown in Figure 4b, the electron is no longer ionized near the peak of the driving field, instead it is ionized from -2.74 to -1.96 o.c., from -1.79 to -0.7 o.c., and from 0.14 to 0.51 o.c. and forms three dominant ionization processes labelled by A_2, B_2, and C_2. The highest-order harmonic is at the 937th order. Compared with the case of the orthogonally chirped two-colour field, since the highest-order harmonic in the two-colour chirped field with the polarization angle of 0.1π is much more higher, the spectral cutoff for the case is greatly extended. The second-highest-order harmonic is at the 205th order, and the third-highest-

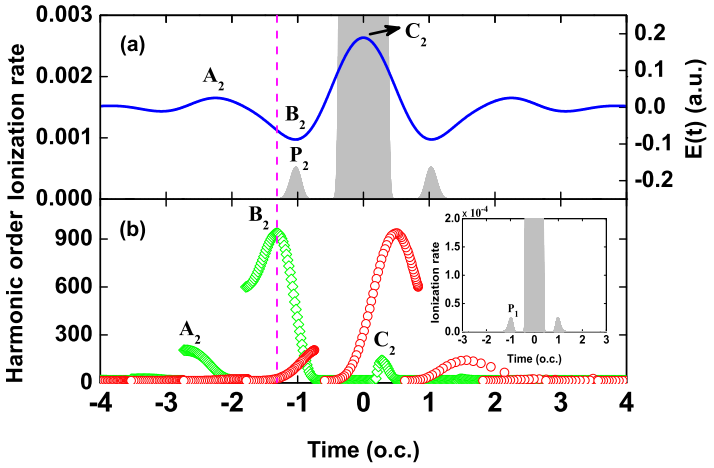

Fig. 4 (colour online). (a) Electric field of y-component of the chirped two-colour field with the polarization angle of 0.1π (solid blue curve) and the ionization rate (gray filled curve). (b) Dependence of the harmonic order on the ionization (green diamonds) and the emission times (red circles). The inset in (b) is the ionization rate in the orthogonally chirped two-colour field. Laser parameters are the same as those in Figure 1.

order harmonic is at the 141st order. In our simulation, the intensity of the laser pulse is much lower than the saturation intensity of the neon atom, the harmonic efficiency is mainly determined by the ionization rate in terms of a three-step model. The contribution of A_2 to the HHG can be ignored due to its extremely low ionization rate. Then the bandwidth of the supercontinuum is directly determined by the energy difference between B_2 and C_2, which leads to a 1236 eV supercontinuum. In addition, we also note that the corresponding ionization rate of B_2, from which the supercontinuum originates, is much lower than that of C_2. Consequently, the harmonic yield of the supercontinuum is several orders of magnitude lower than the lower-order harmonics (i.e., the first plateau), which results in a two-plateau structure in the spectrum. From Figures 4a and 4b, the ionization rate of electrons contributing to the supercontinuum in the chirped two-colour laser field with polarization angle of 0.1π (marked as P_2) is at least one order of magnitude higher than that of electrons in the orthogonally chirped two-colour field, i.e., P_1 (note that P_1 corresponds to the ionization rate of electrons contributing to the continuous harmonics in the orthogonally chirped two-colour field), thereby, the yields of this supercontinuum for this case are much more efficient than that in the orthogonally chirped two-colour field. The above results basically reveal good agreement between the classical theory and quantum time–frequency analysis.

In the following, we investigate the attosecond pulse generation in the chirped two-colour field with the polarization angle of $\theta \leqslant 0.27\pi$. Note that after summing up the intensities of the x- and y-components, the temporal profiles of the generated attosecond pulses can be obtained. For comparison, the temporal profile of the generated attosecond pulse with the orthogonally polarized chirped two-colour field is given in Figure 5a. As shown in this figure, an isolated 104 as pulse is generated by superposing the harmonics from 485th to 510th order, but the duration of the attosecond pulse is wide and the pulse intensity is weak. This is because the harmonic intensity decreases drastically in the cutoff, so that only one or two harmonics effectively contribute to the attosecond pulse. Therefore, the application of the single attosecond pulse for the case is limited. Figures 5b – d present the temporal profiles of the generated attosecond pulses by superposing the harmonics from 400th to 470th order in the chirped two-colour field with three different polarization angles. For the case of $\theta = 0.27\pi$, an isolated 43 as pulse with some weak satellite pulses is produced. The intensities of the weak satellite pulses are below 0.03 of the main peak, so it can be ignored. For the case of $\theta = 0.2\pi$, an isolated 40 as pulse with a clean temporal profile is obtained. For the case of $\theta = 0.1\pi$, a clean isolated 39 as pulse with high signal-to-noise ratio is generated directly without any phase compensation. From these figures above, we can see that isolated attosecond pulses with a duration of about 40 as can be obtained directly for the cases of different polarization angles. This implies that our controlling scheme proposed is suitable for a wide range of polarization angle values, which is favourable for generating a single attosecond pulse with stable pulse duration in experiment. Particu-

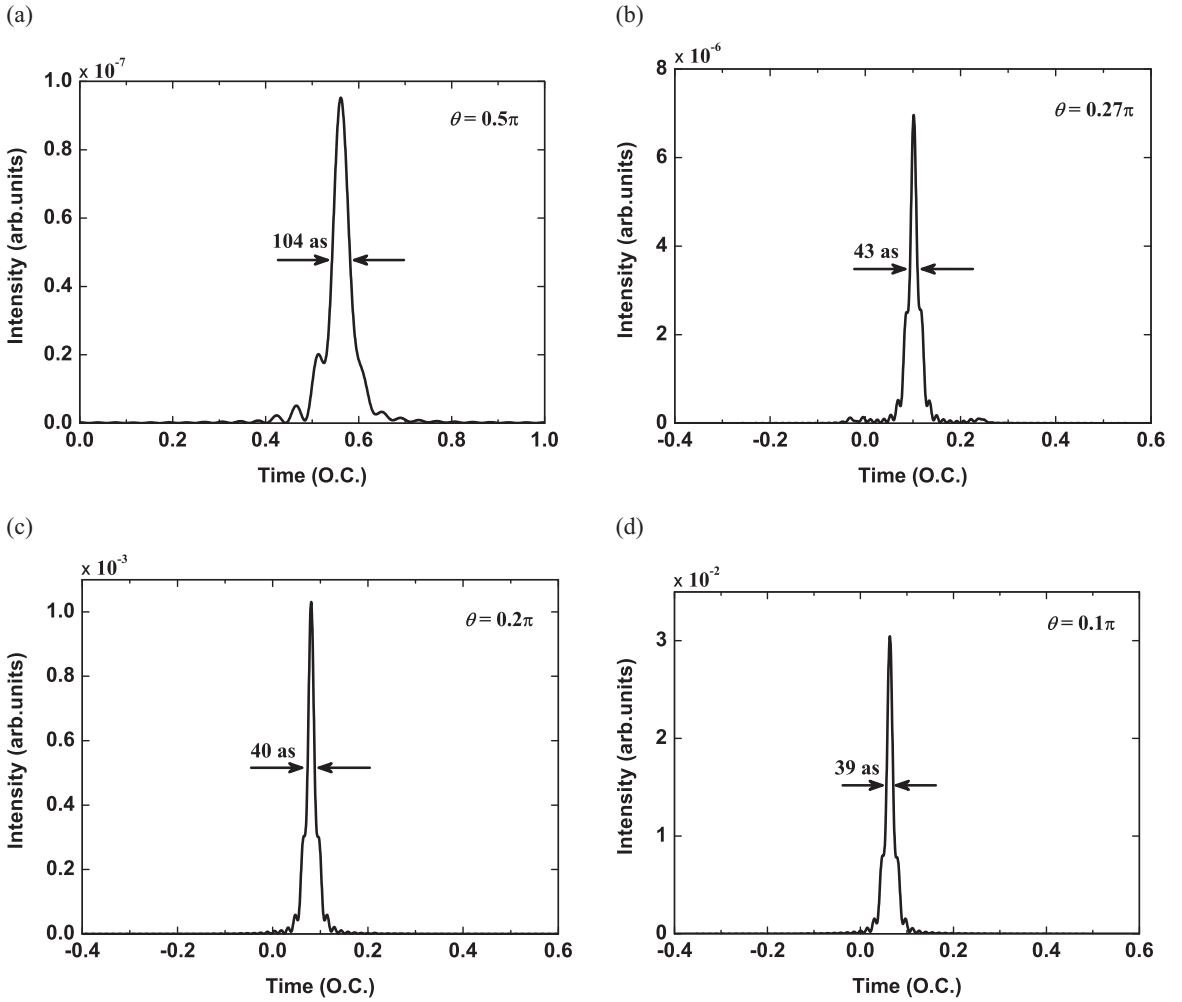

Fig. 5 (colour online). Temporal profiles of the generated attosecond pulses in the chirped two-colour laser field with different polarization angles: (a) 0.5π; (b) 0.27π; (c) 0.2π; (d) 0.1π. Other parameters are the same as those in Figure 1.

larly, we note that the intensity of the single attosecond pulse is enhanced with the decrease of the polarization angle, especially for smaller polarization angle, which lies in the fact that for smaller polarization angle the harmonic efficiency is much more efficient as shown in Figure 2.

In order to clearly show the polarization characteristics of the generated attosecond pulses, we present the three-dimensional plots of the electric fields of the attosecond pulses for the cases of the polarization angle below 0.3π, which are shown in Figures 6a–c. For the case of $\theta = 0.27\pi$, there is a single attosecond pulse with some weak satellite pulses for both for the x- and y-components. With the decrease of the polarization angle, the magnitudes of the electric fields of the x and y components increase, but the magnitude of the electric field of the y-component increases much faster than that of the x- component. For the cases of $\theta = 0.2\pi$ and $\theta = 0.1\pi$, an isolated attosecond pulse with a clean temporal profile for the x- and y-components is obtained, respectively. The above results show that a pure single attosecond pulse for both the x- and y-components is achievable and simultaneously indicate that the generated attosecond pulses are all linearly polarized under the condition of small polarization angle.

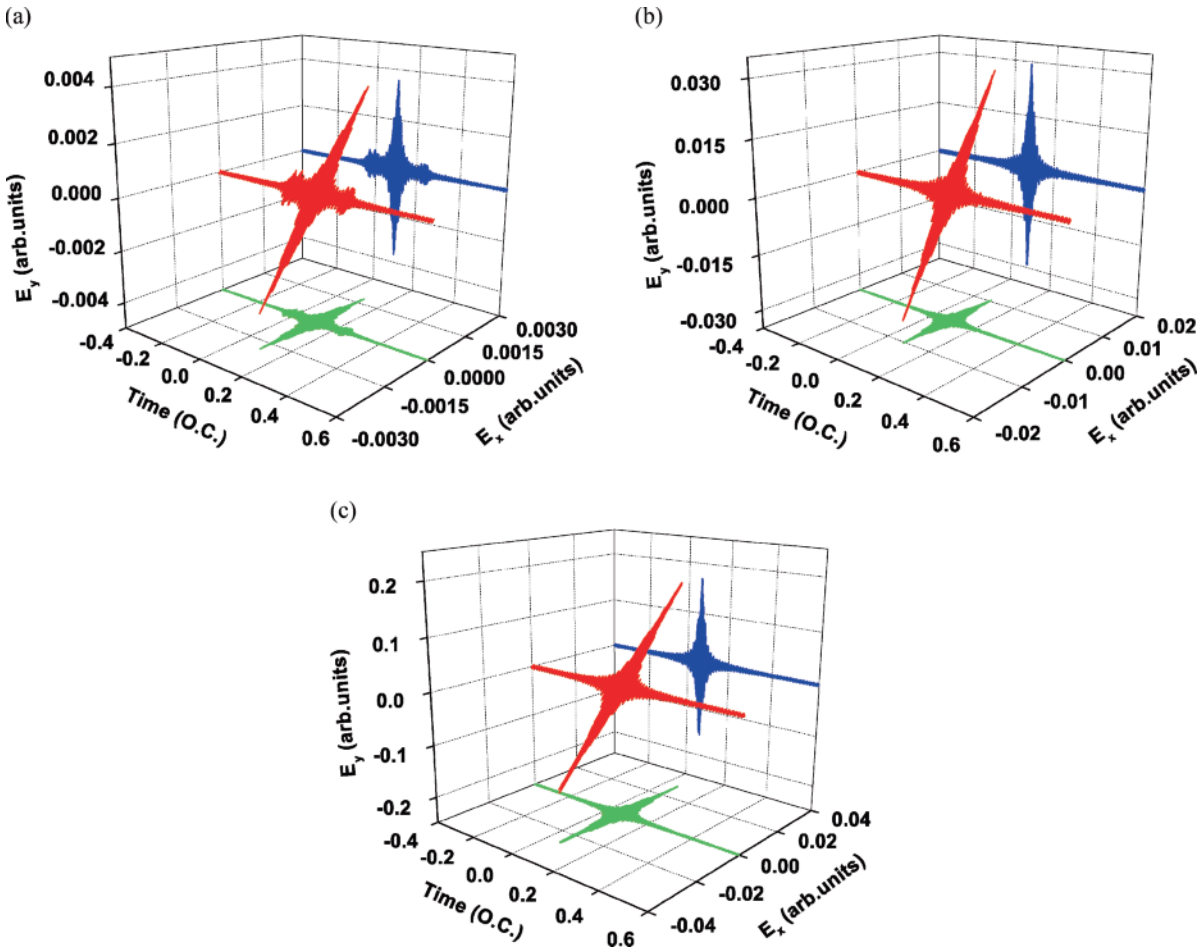

Fig. 6 (colour online). 3D plots of the electric fields of the attosecond pulses for the cases of three polarization angles: (a) 0.27π; (b) 0.2π; (c) 0.1π. Other parameters are the same as those in Figure 1.

In addition, we check how sensitive is the supercontinuum on the chirped parameters β_1 or β_2, respectively. For convenience, here other parameters except for β_1 and β_2 are the same as those in Figure 1. Please keep in mind that in our method the supercontinuum is contributed by the second plateau harmonics. The harmonic spectrum shown in Figure 7a is sensitive to the variation of the parameter β_2. As β_2 increases from 0 to 2, the supercontinuum width is enlarged, and the spectral intensity is enhanced. As β_2 changes from 2 to 4, though the harmonic conversion efficiency decreases, the width of the supercontinuum is significantly extended, particularly for $\beta_2 = 4$, in which the spectral cutoff and the supercontinuum width is the highest. For the case of $\beta_2 > 4$, the supercontinuum spectrum has a low efficiency, especially for the high energy part of the harmonic spectrum, and the spectral cutoff becomes short, which also reduces the bandwidth of the continuous harmonics. Figure 7b shows the harmonic spectra with four different parameter values for β_1. By contrast with the case of $\beta_1 = 6.25$ and $\beta_2 = 4$, no matter whether the parameter β_1 is large or small, the spectral cutoff as well as the harmonic efficiency will decrease, especially for the case of the parameter $\beta_1 \leq 5$. The above results also indicate that the width and intensity of the supercontinuum have a certain degree of dependence on the variation of the parameters β_1 or β_2. But for generating the broadest supercontinuum and maintaining relatively high efficiency, we find that the optimal chirp parameters under the present laser field

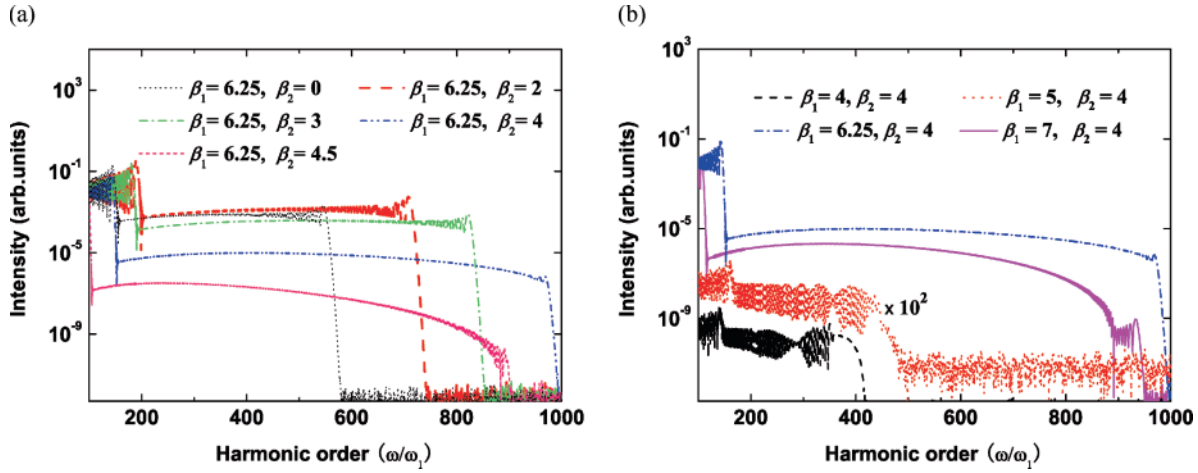

Fig. 7 (colour online). (a) Harmonic spectra with five different parameter values for β_2. (b) Harmonic spectra with four different parameter values for β_1. Note that the harmonic spectrum for $\beta_1 = 5$ and $\beta_2 = 4$ is multiplied by factor of 10^2. Other parameters are the same as those in Figure 1.

are $\beta_1 = 6.25$ and $\beta_2 = 4$, as analyzed above. For the cases of other polarization angles, the dependence of the supercontinuum on the two chirped parameters is the same as the case of $\theta = 0.1\pi$.

We also investigate the influences of the intensities of the two chirped pulses on the supercontinuum. Other parameters are the same as those in Figure 1. Figure 8a presents the harmonic spectra with three different intensities of the 800 nm chirped pulse: $4.0 \cdot 10^{14}$, $5.0 \cdot 10^{14}$, $6.0 \cdot 10^{14}$ W/cm^2, respectively. As shown in this figure, with the increase of the intensity of the fundamental chirped pulse, the first cutoff of the spectrum has almost no change, whereas the second one is markedly enlarged, thus the frequency difference between the first and the second cutoffs is remarkably widened, namely the ultrabroad XUV supercontinuum spectrum appears. The same is true if the intensity of the 1200 nm chirped pulse is increased, as shown in Figure 8b. Just the harmonic cutoff and the bandwidth of the supercontinuum are greatly extended in comparison with that in Figure 8a. Moreover, one can see clearly that the harmonic intensity for above two cases is enhanced. The above results imply that, by properly increasing the intensity of either the fundamental chirped pulse or the subharmonic chirped pulse (exclusive of the case of the depletion of the ground state), not only the spectrum cutoff and the width of the supercontinuum can be extended, but also the harmonic intensity can be enhanced. The unique property offers an opportunity to produce an ultrabroad XUV supercontinuum with high conversion efficiency, which is favourable to the generation of an intense isolated short attosecond pulse. However, since high harmonics are not synchronized on attosecond time scale, selecting the entire available spectral range no longer provides the shortest possible pulses due to the time-phase dispersion, as has been reported in [44]. From our calculation, we find that there exists an optimal bandwidth for the generation of the shortest attosecond pulses in the given conditions of laser parameters, beyond which the pulse lengthens as dispersion dominates [44]. To clarify better, we present the temporal profiles of the generated attosecond pulses for the cases of $I_1 = 6.0 \cdot 10^{14}$ W/cm^2 and $I_2 = 3.0 \cdot 10^{14}$ W/cm^2, respectively. As seen in Figures 8 and 8d, by superposing more harmonics, the attosecond pulse duration lengthens but rather shortens, which best support our point of view.

Finally, we demonstrate that such an effective control scheme can also be extended to the multicycle regime, in which the laser pulse is much easier to achieve in experiment. In this simulation, the driving laser pulse is synthesized by a 20 fs/800 nm fundamental chirped pulse and a 20 fs/1200 nm subharmonic chirped pulse. Other parameters are the same as those in Figure 1. Figure 9 presents our numerical calculated results. As shown in this Figure 9a, the spectrum is smooth and regularly modulated for the har-

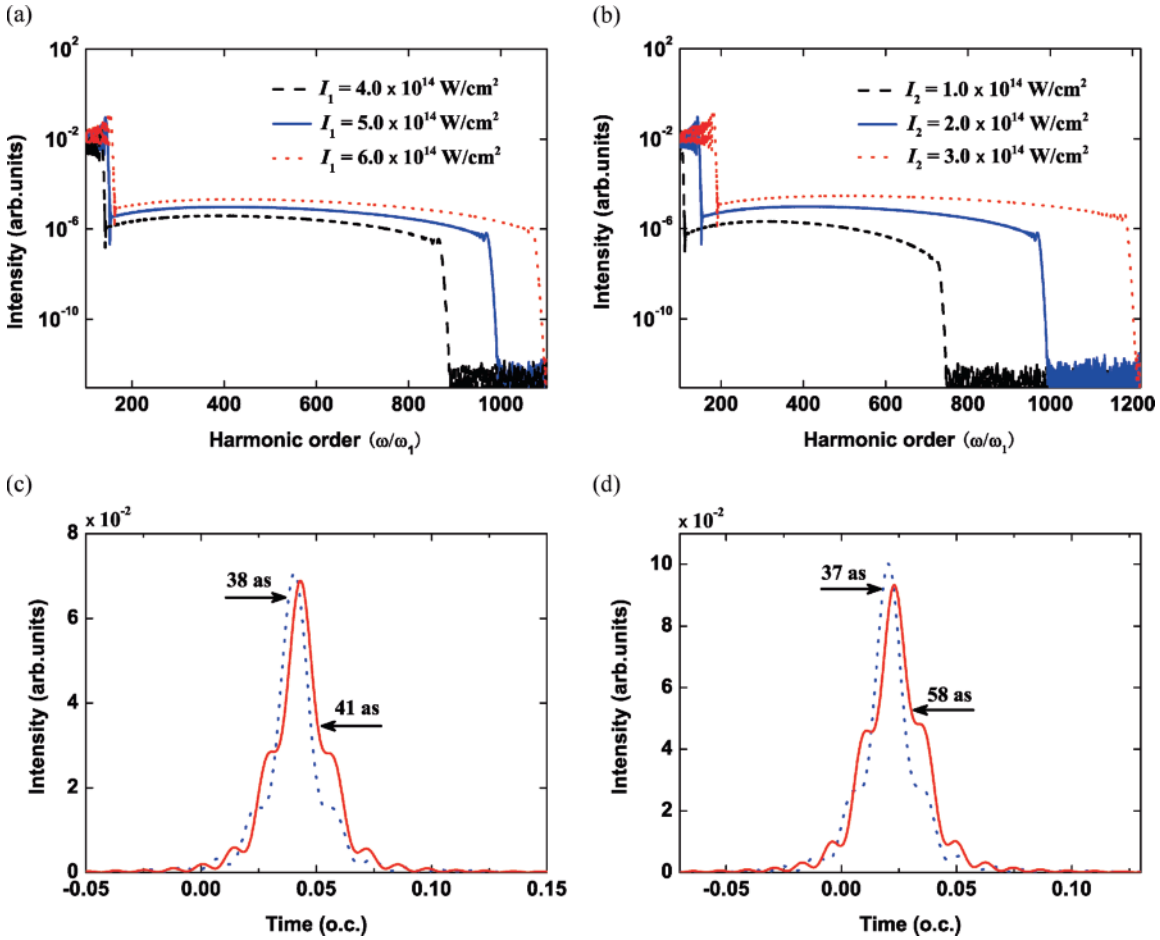

Fig. 8 (colour online). (a) Harmonic spectra with three different intensities of the 800 nm chirped pulse. (b) The same as (a) but for the 1200 nm chirped pulse. (c) Temporal profiles of the attosecond pulses by superposing the harmonics from 400th to 470th (dotted blue curve) and from 400th to 480th (solid red curve) for $I_1 = 6.0 \cdot 10^{14}$ W/cm^2. (d) Temporal profiles of the attosecond pulses by superposing the harmonics from 400th to 475th (dotted blue curve) and from 400th to 485th (solid red curve) for $I_2 = 3.0 \cdot 10^{14}$ W/cm^2. Other parameters are the same as those in Figure 1.

monics from 390th to the cutoff (i.e., $950\omega_1$). Moreover, the harmonic intensity for the case is $1 \sim 4$ orders of magnitude higher than that of the blue curve shown in Figure 2. Figures 9b and 9c present the corresponding time–frequency distributions for the x- and y-components of the HHG spectrum, respectively. Clearly, there are three peaks with maximum orders of 415, 950, and 390 contributing to the harmonics for both components. Since the intensity of the peak A_3 is lower than that of the peaks B_3 and C_3 for both components, the harmonics above 390th order are mainly contributed by the peak B_3, forming an 869 eV XUV supercontinuum. Particularly, for the peak B_3, the intensity of the short path is much higher than that of the long path, i.e., the short-path harmonics is well selected. Thus the harmonics beyond 390th order are almost emitted in phase, i.e., these harmonics are well phase-locked. Since a large range of harmonics which are well phase-locked are produced, a regular single attosecond pulse can be obtained. In order to check this viewpoint, we investigate the attosecond pulse generation in this case. Figure 9d shows the temporal profile of the attosecond pulse by superposing the harmonics from 400th to 470th order. Clearly, a clean isolated 40 as pulse is directly obtained. The duration of the generated single attosec-

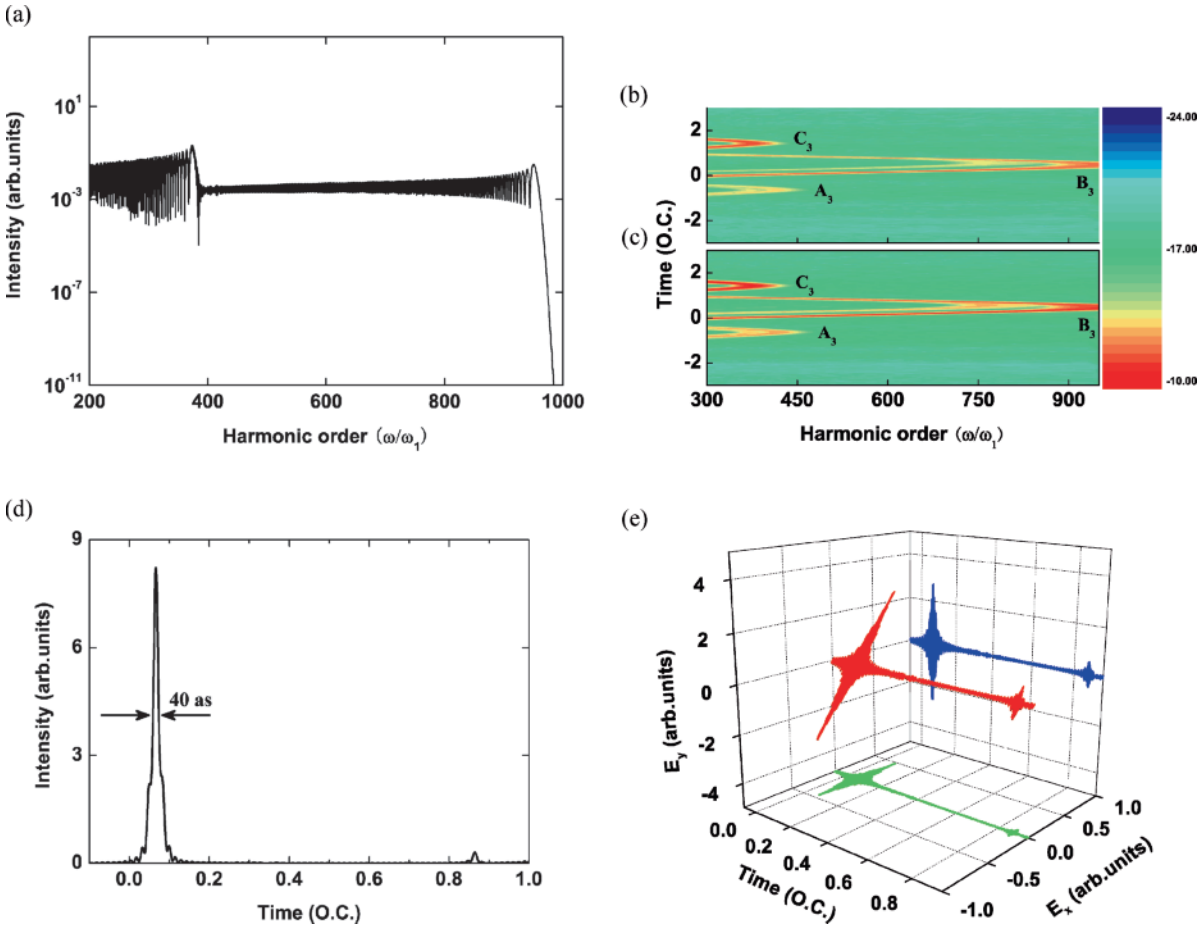

Fig. 9 (colour online). (a) Harmonic spectrum in the chirped two-colour field synthesized by a 20 fs/800 nm chirped pulse and a 20 fs/1200 nm chirped pulse. Time–frequency distributions of the HHG spectrum corresponding to (a): (b) *x*-component, (c) *y*-component. (d) Temporal profile of the attosecond pulse by superposing the harmonics from 400th to 470th order. (e) 3D plot of the electric field of the attosecond pulse corresponding to (d). Other parameters are the same as those in Figure 1.

ond pulse shows almost no change compared with Figure 5d, whereas the intensity of the attosecond pulse is two orders of magnitude higher than that in Figure 5d. Though after the main pulse there is a satellite pulse originating from the long quantum path. The intensity of the satellite pulse only occupies 0.04 of the main pulse, so it can be ignored. In order to clearly show the polarization characteristic of the generated attosecond pulse, we present the 3D plot of the electric field of the attosecond pulse. Figure 9e shows the three-dimensional electric field corresponding to Figure 9d and indicates that the attosecond pulse is linearly polarized.

4. Conclusions

In conclusion, we theoretically investigate the high-order harmonic generation in a synthesized field of a fundamental chirped pulse and a subharmonic chirped pulse. It is show that, by introducing a proper polarization angle, the harmonic cutoff is remarkably extended resulting in an ultra-broad XUV supercontinuum, and the intensity of the harmonic spectrum is effectively enhanced compared with the orthogonally chirped field case. Moreover, by suppressing the long quantum path and enhancing the short one, intense isolated attosecond pulses with a duration of about 40 as

are directly obtained without any phase compensation, which are all linearly polarized. In our method, we show that in a wide range of polarization angle values the broadband supercontinuum with relatively high conversion efficiency can be achieved. Our calculation also shows that the width and intensity of the supercontinuum have a certain degree of dependence on the variation of the parameters β_1 or β_2. But for generating the broadest supercontinuum spectrum and maintaining higher yield, the optimal chirp parameters are $\beta_1 = 6.25$ and $\beta_2 = 4$. Further, the influence of the intensities of the two chirped pulses on the harmonic spectrum is also investigated. The results show that properly increasing the intensities of the two chirped pulses will result in the extension of the harmonic cutoff and the supcontinuum spectrum as well as the enhancement of the efficiency of the supercontinuum (exclusive of the case of the depletion of the ground state). Such an effective control scheme can be extended to the multicycle regime, which makes one facilitate the experimental implement for the broadband isolated attosecond pulse generation. Finally, we would like to point out the feasibility of the scheme. First, an 800 nm laser pulse is available in a good few laboratories, and a 1200 nm laser pulse can be generated by optical parametric amplifier (OPA). Second, the polarization angle between two laser pulses can be experimentally achieved by either the polarizer or the halfwave plate and corresponding polarization splitting prism. Thereby, the scheme presented here appears to be feasible for experimental demonstration in the near future. In brief, the advantage of the scheme proposed lies in generating a broadband XUV supercontinuum with single quantum contribution and high conversion efficiency, which can be used for the production of an intense ultrashort isolated attosecond pulse.

Acknowledgements

This work was supported by the Science Foundation of Baoji University of Arts and Sciences, China (Grant No. ZK11061) and the Education Committee Natural Science Foundation of Shaanxi Province, China (Grant No. 2010JK405 and No. 2013JK0637).

[1] M. Hentschel, R. Kienberger, C. Spielmann, G. A. Reider, N. Milosevic, T. Brabec, P. Corkum, U. Heinzmann, M. Drescher, and F. Krausz, Nature **414**, 509 (2001).
[2] R. Kienberger, E. Goulielmakis, M. Uiberacker, A. Baltuska, V. Yakovlev, F. Bammer, A. Scrinzi, T. Westerwalbesloh, U. Kleineberg, U. Heinzmann, M. Drescher, and F. Krausz, Nature **427**, 817 (2004).
[3] G. Sansone, E. Benedetti, F. Calegari, C. Vozzi, L. Avaldi, R. Flammini, L. Poletto, P. Villoresi, C. Altucci, R. Velotta, S. Stagira, S. D. Silvestri, and M. Nisoli, Science **314**, 443 (2006).
[4] P. B. Corkum, Phys. Rev. Lett. **71**, 1994 (1993).
[5] I. P. Christov, M. M. Murnane, and H. C. Kapteyn, Phys. Rev. Lett. **78**, 1251 (1997).
[6] B. Zeng, W. Chu, G. H. Li, J. P. Yao, J. L. Ni, H. S. Zhang, Y. Cheng, Z. Z. Xu, Y. Wu, and Z. H. Chang, Phys. Rev. A **85**, 033839 (2012).
[7] M. Ivanov, P. B. Corkum, T. Zuo, and A. Bandrauk, Phys. Rev. Lett. **74**, 2933 (1995).
[8] C. Vozzi, F. Calegari, E. Benedetti, S. Gasilov, G. Sansone, G. Cerullo, M. Nisoli, S. De Silvestri, and S. Stagira, Opt. Lett. **32**, 2957 (2007).
[9] C. Altucci, R. Esposito, V. Tosa, and R. Velotta, Opt. Lett. **33**, 2943 (2008).
[10] T. Pfeifer, L. Gallmann, M. J. Abel, P. M. Nagel, D. M. Neumark, and S. R. Leone, Phys. Rev. Lett. **97**, 163901 (2006).
[11] Z. N. Zeng, Y. Cheng, X. H. Song, R. X. Li, and Z. Z. Xu, Phys. Rev. Lett. **98**, 203901 (2007).
[12] P. F. Lan, P. X. Lu, W. Cao, Y. H. Li, and X. L. Wang, Phys. Rev. A **76**, 011402(R) (2007).
[13] W. Y. Hong, P. X. Lu, W. Cao, P. F. Lan, and X. L. Wang, J. Phys. B **40**, 2321 (2007).
[14] C. M. Kim, I. J. Kim, and C. H. Nam, Phys. Rev. A **72**, 033817 (2005).
[15] J. G. Chen, S. L. Zeng, and Y. J. Yang, Phys. Rev. A **82**, 043401 (2010).
[16] E. Goulielmakis, M. Schultze, M. Hofstetter, V. S. Yakovlev, J. Gagnon, M. Uiberacker, A. L. Aquila, E. M. Gullikson, D. T. Attwood, R. Kienberger, F. Krausz, and U. Kleineberg, Science **320**, 1614 (2008).
[17] K. Zhao, Q. Zhang, M. Chini, Y. Wu, X. W. Wang, and Z. H. Chang, Opt. Lett. **37**, 3891 (2012).
[18] G. L. Yudin, A. D. Bandrauk, and P. B. Corkum, Phys. Rev. Lett. **96**, 063002 (2006).
[19] H. Xu, H. Xiong, Z. N. Zeng, Y. X. Fu, J. P. Yao, R. X. Li, Y. Cheng, and Z. Z. Xu, Phys. Rev. A **78**, 033841 (2008).
[20] P. Colosimo, G. Doumy, C. I. Blaga, J. Wheeler, C. Hauri, F. Catoire, J. Tate, R. Chirla, A. M. March, G. G. Paulus, H. G. Muller, P. Agostini, and L. F. DiMauro, Nat. Phys. **4**, 386 (2008).
[21] E. J. Takahashi, T. Kanai, K. L. Ishikawa, Y. Nabekawa, and K. Midorikawa, Phys. Rev. Lett. **101**, 253901 (2008).

[22] T. Popmintchev, M. C. Chen, D. Popmintchev, P. Arpin, S. Brown, S. Ališauskas, G. Andriukaitis, T. Balčiunas, O. D. Mücke, A. Pugzlys, A. Baltuška, B. Shim, S. E. Schrauth, A. Gaeta, C. Hernández-García, L. Plaja, A. Becker, A. Jaron-Becker, M. M. Murnane, and H. C. Kapteyn, Science **336**, 1287 (2012).
[23] J. Tate, T. Auguste, H. G. Muller, P. Salières, P. Agostini, and L. F. DiMauro, Phys. Rev. Lett. **98**, 013901 (2007).
[24] P. Tzallas, E. Skantzakis, C. Kalpouzos, E. P. Benis, G. D. Tsakiris, and D. Charalambidis, Nature Phys. **3**, 846 (2007).
[25] M. Kitzler, X. H. Xie, A. Scrinzi, and A. Baltuska, Phys. Rev. A **76**, 011801(R) (2007).
[26] C. Altucci, R. Velotta, V. Tosa, P. Villoresi, F. Frassetto, L. Poletto, C. Vozzi, F. Calegari, M. Negro, S. D. Silvestri, and S. Stagira, Opt. Lett. **35**, 2798 (2010).
[27] Y. L. Yu, X. H. Song, Y. X. Fu, R. X. Li, Y. Cheng, and Z. Z. Xu, Opt. Express **16**, 686 (2008).
[28] Y. L. Yu, J. J. Xu, Y. X. Fu, H. Xiong, H. Xu, J. P. Yao, B. Zeng, W. Chu, J. Chen, Y. Cheng, and Z. Z. Xu, Phys. Rev. A **80**, 053423 (2009).
[29] W. Y. Hong, P. X. Lu, P. F. Lan, Q. G. Li, Q. B. Zhang, Z. Y. Yang, and X. B. Wang, Phys. Rev. A **78**, 063407 (2008).
[30] J. P. Yao, Y. Li, B. Zeng, H. Xiong, H. Xu, Y. X. Fu, W. Chu, J. L. Ni, X. J. Liu, J. Chen, Y. Cheng, and Z. Z. Xu, Phys. Rev. A **82**, 023826 (2010).
[31] J. P. Yao, Y. Cheng, J. Chen, H. S. Zhang, H. Xu, H. Xiong, B. Zeng, W. Chu, J. L. Ni, X. Liu, and Z. Z. Xu, Phys. Rev. A **83**, 033835 (2011).
[32] J. J. Carrera and S.-I. Chu, Phys. Rev. A **75**, 033807 (2007).
[33] Y. Xiang, Y. P. Niu, and S. Q. Gong, Phys. Rev. A **79**, 053419 (2009).
[34] P. C. Li, X. X. Zhou, G. L. Wang, and Z. X. Zhao, Phys. Rev. A **80**, 053825 (2009).
[35] J. Wu, G. T. Zhang, C. L Xia, and X. S. Liu, Phys. Rev. A **82**, 013411 (2010).
[36] P. Zou, Z. N. Zeng, Y. H. Zheng, Y. Y. Lu, P. Liu, R. X. Li, and Z. Z. Xu, Phys. Rev. A **81**, 033428 (2010).
[37] L. Q. Feng and T. S. Chu. Phys. Rev. A **84**, 053853 (2011).
[38] M. Kitzler, X. H. Xie, S. Roither, A. Scrinzi, and A. Baltuska, New J. Phys. **10**, 025029 (2008).
[39] Th. Udem, R. Holzwarth, and T. W. Hänsch, Nature (London) **416**, 233 (2002).
[40] S. T. Cundiff and J. Ye, Rev. Mod. Phys. **75**, 325 (2003).
[41] M. Lewenstein, P. Balcou, M. Y. Ivanov, A. L'Huillier, and P. B. Corkum, Phys. Rev. A **49**, 2117 (1994).
[42] M. V. Ammosov, N. B. Delone, and V. P. Krainov, Sov. Phys. JETP. **64**, 1191 (1986).
[43] P. Antoine, B. Piraux, and A. Maquet, Phys. Rev. A **51**, R1750 (1995).
[44] Y. Mairesse, A. de Bohan, L. J. Frasinski, H. Merdji, L. C. Dinu, P. Monchicourt, P. Breger, M. Kovačev, R. Taïeb, B. Carré, H. G. Muller, P. Agostini, and P. Salières, Science **302**, 1540 (2003).